JOURNAL OF SPACECRAFT AND ROCKETS
Vol. 42, No. 3, May–June 2005

Nutation Time Constant Determination of On-Axis Diaphragm Tanks on Spinner Spacecraft

Marco B. Quadrelli*
Jet Propulsion Laboratory, California Institute of Technology, Pasadena, California 91109-8099

The modeling, analysis, and testing done to determine the Deep Space One nutation time constant are described. The significance of this analysis and testing program is that Deep Space One was the first spacecraft flown by the Jet Propulsion Laboratory with a diaphragm tank located on the spin axis. First, modeling considerations are made, and to simulate the behavior of the spacecraft containing the liquid (hydrazine) the dynamics of a rigid body coupled through a universal joint to a pendulum mass representing the liquid slosh has been analyzed. This simulation is done in order to estimate the nutation time constant with a pendulum slosh model. Second, the actual spin drop tests are described. These tests also confirm a nutation time constant in excess of 1000 s, both in the case of tests done for the xenon tank only and in the case of tests done for the hydrazine tank only. The large value of the nutation time constant computed and verified by testing for this system ensured that it remained well above the required values of 150 s at ignition and 50 s at burnout.

Nomenclature

A	=	acceleration, m/s^2
A_{ij}, B_{ij}	=	dimensionless parameters
a_t^k	=	linear acceleration remainder terms
B	=	base body (spacecraft)
B^+	=	spacecraft center of mass
Bo_E	=	elastic Bond number
$\boldsymbol{b}_i$	=	unit vectors, $i = 1, 2, 3$
C_{ij}, D_{ij}	=	nondimensional coefficients depending on the Poisson's ratio
c	=	damping coefficient for the slosh pendulum, N-s/rad
c_d	=	membrane damping coefficient, N-m/s
c_i	=	arbitrary constants
d	=	tank diameter, m
E, E_1, E_2	=	modulus of elasticity of the inner (outer) layer of the shell, N/m^2
F_k	=	vectrix of rigid body, where k denotes the body index
F_{ij}	=	internal force resultants, N
F_t^k, F_e^k	=	generalized inertia and external forces, N
Fr_f	=	Froude number
G	=	energy dissipation rate per unit time
g	=	external acceleration field, m/s^2
H, H_1 (H_2)	=	thickness of inner (outer) layers of composite shell, m
h	=	liquid level, m
$\boldsymbol{h}$	=	hinge point location with respect to the bus center of mass, m
I, I_1, I_2	=	transverse moment of inertia, kg-m^2
J	=	spin moment of inertia, kg-m^2
k	=	stiffness coefficient for the slosh pendulum, N/rad
l_h	=	hinge point location from tank bottom, m
l_s	=	pendulum length, m
l_0	=	rest mass location, m
M_{ij}	=	internal moment resultants, N-m
m_f	=	fluid mass, kg
m_{full}	=	mass of full tank, kg
m_s	=	moving (slosh) mass, kg
m_t	=	effective mass, kg
m_0	=	rest mass, kg
N	=	inertial reference frame
n_θ, n_φ	=	viscoelastic reaction torques, N-m
O	=	reference point in B
P	=	slosh mass
p	=	fuel pressure, N/m^2
$\boldsymbol{q}$	=	unit Euler parameters (quaternion)
R	=	tank radius, m
Re_E	=	elastic Reynolds number
${}^Q\boldsymbol{r}^P$	=	position vector of P with respect to Q, m
S	=	tank shape factor (spherical, cylindrical, etc.)
T_e	=	external torque on pendulum, N-m
T_t^k, T_e^k	=	generalized inertia and external torques, N-m
$\boldsymbol{u}$	=	vector of generalized speeds
V	=	velocity of sound in fluid, m/s
${}^N\boldsymbol{v}^B$, ${}^N\boldsymbol{v}^O$, ${}^N\boldsymbol{v}^P$	=	linear velocity of B, O, P, m/s
${}^N\boldsymbol{v}_r^B$, ${}^N\boldsymbol{v}_r^Q$, ${}^N\boldsymbol{v}_r^P$	=	partial linear velocities, $r = 1, \ldots, 8$
z	=	axial offset of tank center from spacecraft center of mass, m
α, β, γ	=	nondimensional scaling ratios
α_t^k	=	angular acceleration remainder terms
Γ_d	=	shell shear stiffness, N/m
ε_{ij}	=	strain components in the plane tangent to the middle surface of the shell
ζ	=	thickness variable, m
η	=	structural deflection, m
θ	=	pendulum in-plane angle, rad
θ, θ_0, θ_f	=	nutation angle, rad
Λ_d	=	shell extensional stiffness
λ	=	nutation frequency, rad/s
μ_f	=	fluid dynamic viscosity, kg/ms
ν	=	Poisson's ratio
ν_f	=	kinematic viscosity, m^2/s
ρ_d	=	structural density, kg/m^3
ρ_f	=	fluid density, kg/m^3
Σ_d	=	shell bending stiffness, Nm
σ, σ_{eq}, σ_1, σ_2	=	inertia ratio
σ_{ij}	=	stress components, N/m^2

Presented as Paper 2003-0155 at the AAS/AIAA 13th Spacecraft Mechanics Meeting, Ponce, PR, 9–13 February 2003; received 8 September 2003; revision received 7 April 2004; accepted for publication 7 April 2004.

*Senior Engineer, Mail Stop 198-326; marco@grover.jpl.nasa.gov. Senior Member AIAA.

τ, $\tau_{\text{fullscale}}$, τ_{model} = represents the nutation divergence time constant, s
τ_r = generalized forces, N
φ = pendulum out-of-plane angle, rad
Ω = spin rate, rad/s
ω_{BN} = body nutation frequency rate, rad/s
ω_{IN} = coning rate, rad/s
${}^N\boldsymbol{\omega}_r^B$, ${}^N\boldsymbol{\omega}_r^P$ = partial angular velocities, $r = 1, \ldots, 8$
ω_s = slosh frequency, rad/s
ω_T = transverse rate (tip-off rate), rad/s
ω_0 = undamped frequency, rad/s
ω_{1g} = slosh frequency for 1-g conditions, rad/s
${}^N\boldsymbol{\omega}^B$ = angular velocity of B, rad/s

Introduction

THE nutation time constant (NTC) estimate is required for launch vehicle stability analysis. This time constant is involved in any launch with a spinning upper stage for injection. The divergence time constant is a significant input to the nutation control system analysis and establishes the initial cone angle at third-stage ignition; it contributes to the velocity pointing and loss during motor burn and establishes the cone angle at the start of spacecraft separation. The Deep Space One (DS1) spacecraft, shown in Fig. 1, utilized a monopropellant hydrazine blowdown propulsion system for attitude control and trajectory correction maneuvers. This system incorporates the use of one spherical, 16.5-in.-diam titanium propellant tank. This tank is mounted on the $+Z$ axis of the spacecraft and incorporates a flexible elastomeric diaphragm for propellant control/management. Because of the configuration of the tank on the spacecraft, because the spacecraft is spinning at 62.8 rpm at thruster ignition, and because of the nature of the diaphragm, it is important to evaluate the influence of this particular topology on the nutation divergence time constant of the spacecraft when energy dissipation due to liquid motions is possible.

The case of the Exosat spacecraft,[1] which was a spinner with an on-axis diaphragm tank, is significant and very relevant to the subject of this paper: analysis showed that adding the diaphragm decreased the divergent nutation time constant by a factor of 6–7 relative to a bare tank. However, the diaphragm configuration was different than in DS1 and more prone to static and dynamic instability. The conclusions of Marce's report[1] concerning the responsibility of inertial wave resonances on the nutation instability of Exosat have been questioned based on the fact that there is no correlation between the Exosat test results and the pretest predictions[2–4] (also because the predictions did not take into account the increased damping effects caused by the presence of a flexible diaphragm). Recent studies of the nutation time constant of the Deep Impact spacecraft,[5] with two on-axis hydrazine tanks of different dimensions, also conclude that the liquid-induced resonances (and perhaps the nutation synchronous mode described next) can also appear during the preburn and postburn phases.

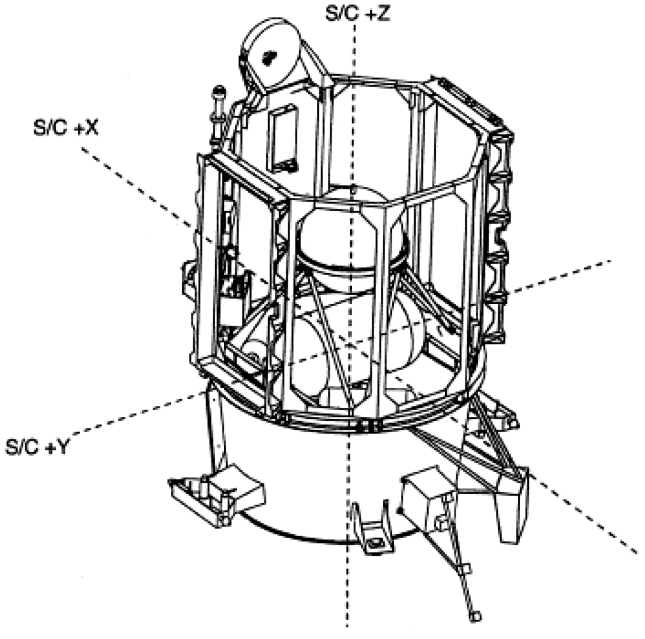

Fig. 1 Configuration of the DS1 spacecraft.

This paper describes the challenges of the problem under investigation, discusses modeling approaches, presents a slosh pendulum analysis done to support the study of the effect of an elastomeric diaphragm located inside an on-axis spinning tank, and discusses the testing done to support the modeling and analysis. The forces and torques acting on the structural system depend on the pressure distribution on the liquid container walls. On the other hand, the current distribution of vorticity (as well as velocity and pressure) in the body of fluid depends on the current distribution of linear and angular accelerations to which the base vehicle is subjected. The nutation characteristics of the whole system also depend on the dissipation induced by the liquid viscosity, as well as on the presence and damping characteristics of propellant management devices (baffles, membrane diaphragms, or others). Besides the nutation, spinning bodies are also subject to a wobble amplification phenomenon, which depends on the hydrostatic distribution of the liquid with respect to the vehicle's principal axes. Energy dissipation in spinning bodies containing liquids generally depends on tank shape and geometry (spherical, conospherical, cylindrical, isotensoid), tank fill fraction (FF), propellant management device (PMD) shape and viscoelastic properties (shape, orientation in tank, material constants), PMD orientation in on-centerline (CL) or off-CL tank, tank location with respect to vehicle centerline and center of mass, interaction with moving center of mass (during burn), and vehicle inertia ratio (spin to transverse inertia).

After a section reviewing the main features of the physics of liquids within spinning spacecraft, a following section describes the simulation model used for the DS1 nutation time constant determination. Next, the spin drop test program is described, together with a discussion of the nutation testing results, and a brief section summarizing the telemetered flight data concludes the paper.

Physics of Liquid-Wall Interaction with and Without Diaphragm

We will begin with some general considerations, following Harrison's paper.[6] An understanding of the most general case of spinning body dynamics, including the effects of initial transverse rates, dynamic unbalance, asymmetry, and internal energy dissipation, can best be achieved by means of simple examples. Consider a symmetric, cylinder-like, and dynamically balanced spinning rigid body under no external torques. A quantity of interest in the following considerations is the inertia ratio $\sigma = (J/I)$. For an asymmetric body, that is, one in which the transverse moments of inertia I_1 and I_2 are unequal, one makes use of the equivalent inertia ratio $\sigma_{\text{eq}} = 1 - \sqrt{[(\sigma_1 - 1)(\sigma_2 - 1)]}$, where $\sigma_1 = [J/(I_1)]$ and $\sigma_2 = [J/(I_2)]$. Because there are no external torques, the body's angular momentum is fixed in space. The pure spin case is the situation in which the body spins with a body-fixed axis coincident with the angular momentum vector. If a transverse rate ω_T (tip-off rate) exists, the resulting motion is called nutation: the body-fixed symmetry axis cones around the angular momentum vector. The half-cone angle $\theta = \tan^{-1}(\omega_T/\sigma\Omega)$ is called nutation angle. The coning rate $\omega_{\text{IN}} = \sigma\Omega$ is called the inertial nutation frequency. When the observer sits in the body, the instantaneous axis of transverse angular velocity rotates around the body-fixed desired spin axis at the body nutation frequency rate $\omega_{\text{BN}} = (\sigma - 1)\Omega$. This rotation is retrograde if $\sigma < 1$; it is prograde if $\sigma > 1$. This rotating angular velocity causes sinusoidal accelerations within the body, which cause centrifugal loading on flexible structural elements, liquids, structural connections, dampers, or sensitive instruments such as accelerometers or other sensing equipment. The forcing frequency is the body nutation frequency, which depends only of the spin speed and the inertia ratio. A point at a distance d from the spin axis is then subjected to an acceleration $A = \sigma(2 - \sigma)d\Omega^2 \tan\theta$. Finally, it is well known that a prolate spinner is unstable, that is, if the ratio of the spin to

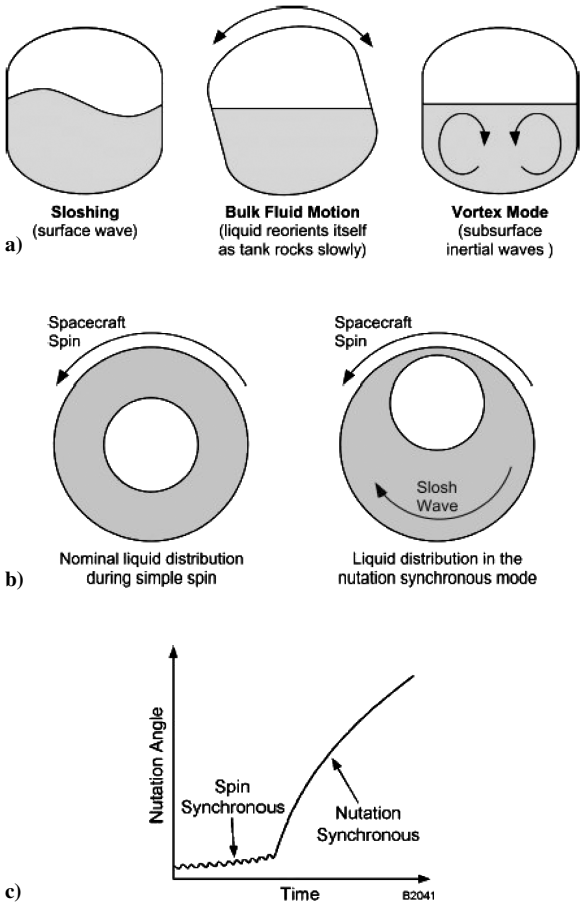

Fig. 2 Modes of fluid motion in tanks: a) typical, b) spin-synchronous vs nutation-synchronous mode, and c) nutation angle of spin-synchronous vs nutation-synchronous mode vs time (courtesy of Carl Hubert of Hubert Astronautics, Inc.).

transverse moment of inertia is less than one, and the body is spinning about the axis of minimum moment of inertia, an initially small nutation angle θ_0 will increase in a finite time Δt to θ_f according to the equation $\theta_f = \theta_0 \exp(\Delta t/\tau)$.

In a fluid-structure interaction problem there are three different modes of fluid motion.[3,7,8] Stewartson's paper[9] provides an analytic procedure for calculating the eigenmodes and nutation rates for a spinning body with a cylindrical cavity with flat end walls containing an inviscid liquid, showing that a doubly infinite series of eigenmodes and frequencies appears. Stewartson's paper[9] also provides the seed for further research, including Wedemeyer's paper,[10] which provides viscous corrections to Stewartson's theory that brought about better agreement with experimental observations of the resonant frequencies for specified cavity aspect ratios. We refer to Fig. 2 and proceed to summarize the essential features of this dynamic interaction.

Bulk Motion Mode

In the bulk motion mode (Fig. 2a), a motion exists that denotes a condition of hydrostatic equilibrium of a contained liquid under the influence of a conservative, external acceleration or body force field (such as gravity or centrifugal acceleration exerted under a condition of steady, uniform rotation of the tank about a fixed axis). The adjustment of fluid to a state of hydrostatic equilibrium in a spinning tank is important from the standpoint of establishing a reference condition from which nutational perturbations can be measured, and it will produce wobble angle amplification if there is a seed dynamic imbalance in the mass properties of the rigid spacecraft. Bulk fluid motion is characterized by liquid reorienting itself within a tank in response to changes in the tank's alignment relative to the acceleration field and/or inertial space. Nutation produces a cyclic bulk motion that dissipates energy as a result of viscous drag as the liquid flows past the tank walls and diaphragm. When the liquid is in a state of uniform rotation in a spinning tank, it is endowed with vorticity with respect to the inertial frame (where the vorticity is equal to twice the angular velocity), and any flow relative to the tank will not be irrotational. For a simple spherical tank, bulk motion can be modeled by treating the liquid as a solid body that pivots about the center of the tank. Accurate mechanical analogs are more difficult to develop for nonspherical and diaphragm tanks. Figure 2c shows that the nutation synchronous mode is excited in a different manner than the conventional spin-synchronous mode. The bulk motion in tanks with internal devices can dissipate a lot more energy than in bare tanks. In fact, the diaphragm causes the fluid-filled spherical cavity to become nonspherical, resulting in a vigorous fluid motion initiated by the viscous boundary layer at the tank walls. In the case of a partially filled cavity, the diaphragm assumes a grossly wrinkled shape, which differs from the bare tank free surface. Because the diaphragm causes the fluid-filled cavity to be nonspherical, the liquid motion will dissipate more energy on account of a more complex velocity distribution than in a bare tank.

Sloshing Mode

The sloshing mode (Fig. 2a) occurs when the liquid has a free surface and involves liquid motion in a direction perpendicular to the free surface with very little or no circulation. The determination of the sloshing oscillations of a fluid in an axisymmetric tank consists of a solution for the velocity potential described by Laplace's equation in three dimensions, which satisfies the prescribed tank wall and boundary conditions and free-surface boundary conditions. From this solution, the equations for the hydrodynamic pressures, forces, moments, surface waveforms, and natural frequencies can be obtained. A simple mechanical analogy in the form of a pendulum or equivalent spring mass will exactly duplicate the forces and moments produced in the fluid oscillations. Physically, the motion of the fluid can be interpreted as follows. A certain portion of the liquid can be considered as rigid and not participating in the sloshing motion, whereas the fundamental mode reacts as a pendulum and can oscillate as such. The higher modes are not important, as the sloshing masses participating in the motion become smaller as the natural frequency increases. Because the fluid is generally assumed to be incompressible and inviscid, the mechanical analogy does not apply well in situations in which the predominant source of internal recirculation is viscous friction at the tank walls or at the diaphragm surface.

In a spherical diaphragm tank with ullage over the liquid, the diaphragm reduces the wavelength of the slosh mode, increases the frequency, and results in a similar mode shape to the case with the bare tank. The slosh mode frequency and damping ratio increase with diaphragm thickness, and because of the diaphragm viscoelasticity the free-surface slosh mode is highly damped. The determination of diaphragm viscoelasticity and its effects on this mode are very important.

Nutation Synchronous Mode

A different mode of motion is the nutation synchronous mode,[3,11–14] which involves a unidirectional (noncyclic) surface wave that revolves around the spin axis at the nutation frequency. The difference in nutation growth characteristics under the influence of simple oscillatory spin-synchronous motion and the more vigorous nutation-synchronous motion is shown qualitatively in Figs. 2b and 2c. We only mention it to complete the description of possible modes of liquid motion in a spinning spacecraft. On-axis tanks can also support this type of nonoscillatory liquid motion. With an inertia ratio of about 0.2, with a spin rate of 60 rpm, this nutation synchronous wave would circulate around the spin axis at over 40 rpm in a direction opposite to the spin. Such a high velocity flow can dissipate significant amounts of energy and cause rapid nutation growth. A vehicle that experienced this type of behavior is the IMAGE spacecraft,[3] which had no liquid propellant but did have a passive viscous-ring nutation damper that contained 1.2 kg of mercury. To excite nutation-synchronous behavior requires a minimum nutation amplitude. This critical angle is a function of several

parameters, including spin rate, inertia ratio, tank radius, distance from the vehicle cm to the tank center, amount of moving liquid, and effective damping coefficient. If the effective damping coefficient is low enough and/or the moving mass is high enough, then the critical angle for exciting nutation-synchronous motion will be within the range of angles that could be experienced in flight. As indicated by the IMAGE experience,[3] nutation-synchronous motion can cause very rapid nutation growth. Because nutation synchronous behavior is nonlinear, it cannot be analyzed with eigenvalue methods resulting from pendulum models. It is unknown if this type of motion was observed in the Deep Space One spacecraft.

Inertial Waves

Inertial wave modes are a dissipative mechanism, which can occur only in spinning tanks, are independent of the presence of a free surface, and can couple with nutation motion. Inertial waves can be excited in nonspherical tanks and are the result of redistribution of the fluid initiated at the tank walls, progressively diffusing inside the spinning liquid, and these modes have a sectorial character. Inertial waves are driven by the cyclic pressure waves from nutation-induced, angular motions of the tank wall coupled with Coriolis forces inside the liquid. Inertial wave resonances can occur within a bandwidth of two times the spin rate for a prolate spinner, and they can be identified by producing one or more sharp peaks in a plot of the energy dissipated by the liquid in a spinning spacecraft vs inertia ratio. Because of the sharp energy dissipation that they can produce, the nutation time constant can be drastically reduced if the configuration of the spacecraft is such that the resonance can occur.

As stated in Vanyo's book,[15] a rotating fluid supports inertial waves if it is Rayleigh stable, that is, if the angular momentum per unit mass of the circular flow lines increases with the radius from the spin axis. The Rayleigh criterion asks whether the force caused by inward radial pressure gradient is adequate to maintain an inward centripetal acceleration for a generic element of the fluid in that rotating flow. If the criterion is satisfied, that is, if the flow is stable to perturbations, then fluid elements moving radially out or radially inward will tend to return to their initial radius when the perturbation has ceased. Unless the flow is heavily damped (i.e., if baffles are present or the fluid is highly viscous), the element of perturbed fluid will overshoot from the undisturbed radial position and initiate an oscillatory wave motion called the inertial wave.

Miles[16] and Miles and Troesch[17] show when free-surface sloshing and inertia waves might occur in tanks of different shapes, although there is no unified treatment of the subject that can be applied to tanks of all possible shapes. Inertial waves (Fig. 2a) give rise to natural modes and frequencies within the contained, rotating fluid. Resonance occurs when the fluid motion is excited (by an oscillatory motion of the tank, for example) at a frequency that is close to one of the natural frequencies of the fluid. They are traveling and also dispersive solutions of a hyperbolic equation,[8] which implies that discontinuities can occur in the fluid across characteristic surfaces (cones). These waves die out in a time of the order of the spin-up time (roughly proportional to the square root of the Reynolds number). In a sphere, for example, the first inertial mode is a spin of the interior fluid about a single axis as if it were a rigid body. Higher modes are obtained by seeking smaller subdivisions of the sphere with corresponding motions that satisfy both continuity and momentum balance. In a clean fully filled spherical tank, the only fluid-structure interaction mechanism is at the viscous boundary layer at the tank wall. Inertial waves can occur in fully loaded tanks, with 100% fill factor. Slosh resonances are generally excited[18] in (forced motion spin table) tests driven at low spin rate (<30 rpm) and high nutation rate (>80 rpm). Conversely, inertial wave resonances, if they exist, should generally be excited in tests driven at large spin rates (>60 rpm) and small nutation rates (<40 rpm). Zedd and Dodge[18] use a rotor model with a viscous damper to model the boundary-layer dissipation and the inertial wave resonance.

Unlike the modal decomposition of an elastic member, a spinning fluid does not have a lowest frequency mode and a modal structure in which the frequencies progressively march up from the lowest value to infinity. Rather, the eigenvalues tend to cluster in the interval $[-2\Omega, 2\Omega]$, where Ω is the spin rate with numerous excursions outside this interval when a free surface is present.[8,13] Hence, the fluid modes cannot be ordered according to the magnitude of the eigenvalue. Instead, this ordering is based on the number of nodal surfaces that a particular mode has.

To excite these inertial wave modes, energy must be introduced into the flow. For a clean sphere, the excitation can originate at the viscous boundary layer with the tank walls. For a nonspherical surface, the forcing function also includes normal velocities of the boundaries relative to the fluid mass. When there is structural symmetry, solutions can be expressed in terms of Legendre polynomials or Bessel functions, which typically represent axisymmetric expansions. Once excited, the inertial waves move both axially and radially, producing conical shear surfaces, which can be visualized in the laboratory using transparent tank walls and tracers in the illuminated liquid. In general, one could say that inertial resonances are extremely sensitive to changes in system geometry.

In a clean spherical tank, the only fluid-structure interaction mechanism is at the boundary layer at the tank wall, sustained by viscous shear. Previous experiments done with water and mercury on a nonspinning tank with 16.5% ullage (83.5% filled)[19] show that the slosh response was found to be very dependent on the stiffness and deformed shape of the tank positive expulsion diaphragm, for tests done under horizontal excitation. The diaphragm altered the free surface of the fluid by supporting the fluid away from the tank walls. As a result, the classic first free-surface slosh mode, which is represented by a fluid pendulum motion, does not occur. Therefore, the system stiffness appeared to be almost entirely controlled by the stiffness and shape of the diaphragm. In addition, it was also established[19] that a single multiple-degrees-of-freedom pendulum model could not be assumed across the entire frequency range of operation for the tests, rather different models had to be used in different frequency ranges.

A report by Dodge on the NEAR spacecraft,[2] which had a spinning tank with a similar on-axis tank configuration with diaphragm, presents some of the issues of interest in the model. Because the tanks are located on the spin axis, spinning simply causes the propellant and diaphragm to be oriented in an axisymmetric shape about the spin axis. No significant lateral shifting of the spacecraft center of mass from the axis was expected. Given the absence of internal hardware, the viscous stresses at the walls are the only available mechanisms to cause the liquids to rotate. There is a very complicated transient liquid flow pattern during spin up, caused by growing boundary layers, internal recirculation flows, and tank end effects.

In general, the presence of a diaphragm inside a fuel tank adds a significant uncertainty to the vehicle dynamics of a spinner spacecraft. One remarkable case was EXOSAT (another spinner spacecraft with on-axis tank with diaphragm), in which tests showed that the major sources of dissipation were the internal modes and not the free-surface slosh modes, that the effect of the diaphragm orientation inside the tank is crucial for determining the onset of nutation, and that adding diaphragms to the propellant tanks decreased the divergent nutation time constant by a factor of six or seven relative to the bare tank. Generally, to ensure success the configuration to be flown must lie within the parameter space of previously tested or flown configurations, the reason being that there is a significant sensitivity to parameter variations (fill fraction, tank shape, inertia ratio, etc.). Figure 3 depicts the grossly deformed diaphragm of a hydrazyne tank used for the Mars Polar Lander spacecraft at different fill factors. Figure 3 shows some modes of deformation of an elastomeric diaphragm inside a draining tank, obtained from a recent report.[20] The analysis in Kreis et al.'s paper,[20] although quite detailed and promising, is limited to small deformations of an elastomeric diaphragm, under gravity and large material rigid body rotations, and the fluid contribution is obtained from pressure equilibrium in a 1-g field only.

Pendulum Models

The pendulum model is routinely used by the aerospace industry to provide a solution to the slosh problem to first order of approximation. Unfortunately, it can be useful only to roughly estimate

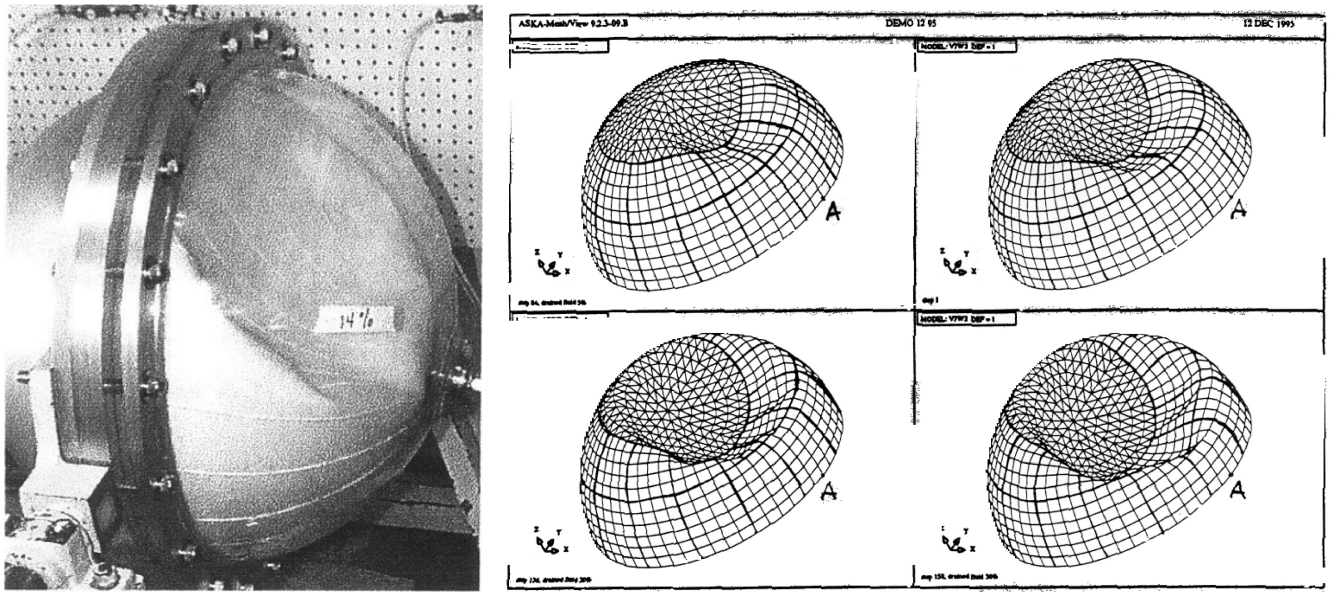

Fig. 3 Mars Polar Lander test of tank with diaphragm (left) and modes of deformation of an elastomeric diaphragm inside a draining tank (right) (from Ref. 14).

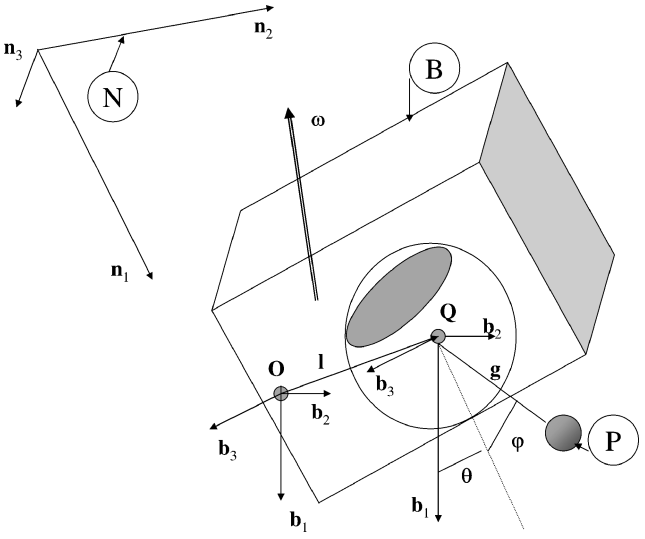

Fig. 4 Mechanical model used for nonlinear time simulation.

the nutation divergence time constant, and it is not useful for accurate predictions. Traditionally, analytical (pendulum) models often grossly underestimate the severity of the resonances occurring in the fluid-structure interaction process. The presence of a PMD introducing dissipation into the attitude dynamics of the vehicle is modeled in the pendulum model via a rotary stiffness and damping coefficient, thereby providing a linear viscoelastic model of a pendulum as in Fig. 4, where the motion of the conical pendulum is restrained by a rotational spring and a damper. As just stated, the determination of the forced oscillations of a fluid in a tank of axisymmetric shape consists of a solution for the velocity potential described by the Laplace equation in three dimensions, which satisfies the prescribed tank wall and boundary conditions and free-surface boundary conditions. Once this solution has been obtained, the equations for the hydrodynamic pressures, forces, moments, surface waveforms, and natural frequencies are combined to compute the effects of the variation in velocity potential. The mechanical analogy in the form of a pendulum or equivalent spring mass will exactly duplicate the forces and moments produced in the fluid oscillations, up to any order in a series expansion of the velocity potential.[21,22] The physical equivalence consists in having a certain

Table 1 Mass and geometric parameters of the Deep Space One spacecraft for different center-of-mass locations

Parameter	Preburn	Postburn
Vehicle's c.m. location, m	0.265, 0.261	0.265, 0.261
Mass, kg	1717.7	643.6
Inertia ratio	0.223, 0.231	0.321, 0.330
Tank center/c.m. offset, m	1.39, 1.40	0.645, 0.675

portion of the liquid that can be considered rigid and not participating in the sloshing motion, whereas the fundamental sloshing mode reacts as a pendulum and can oscillate as such. As in any modal analysis, the higher sloshing modes participate in the motion with increasingly smaller amplitudes as the natural frequency increases. One drawback of the pendulum models for sloshing only is its ineffectiveness in capturing internal recirculation dynamics because the fluid is generally assumed to be incompressible and inviscid. Consequently, the mechanical analogy does not apply well in situations where the predominant source of internal recirculation is viscous friction at the tank walls or at the diaphragm surface.

Derivation of Pendulum Model Parameters

The STAR 37 FM motor and DS1 spacecraft are spin stabilized (nominal spin rate = 62.8 rpm); the spherical hydrazine tank (radius = 0.209 m) is located on the spin axis, directly above the xenon tank; the hydrazine tank contains a flexible diaphragm as a propellant management device; and the required minimum nutation time constants are 150 s at ignition and 50 s at burnout. At launch, the fill level of the equivalent clean tank, that is, a tank of the same radius as the tank in DS1, but without diaphragm, is 87.5%. The liquid mass in the tank is 27.8 kg. The mass properties of the whole third-stage vehicle (DS1 attached to the STAR37 solid rocket motor) are given in Table 1. The nominal spin rate of the full scale vehicle is 60 rpm, and the nominal inertia ratios are 0.222 (preburn) and 0.296 (postburn). The tank center location is nominally at 0.5154 m from the reference plane, on the spin axis. The hydrazine tank contains a diaphragm of thickness 1.651 mm, made of an elastomer with Young's modulus equal to 8.4368×10^5 kg/m^2.

The diaphragm is made of AF-E-332, which is a relatively stiff elastomer. Although this material can be stretched to 300% of its original length in a uniaxial test, in its implementation the diaphragm can only stretch 10% before failing. The diaphragm in this state provides a semistiff control surface and is resistant to deformation.

Filling of the tank occurs with the diaphragm originally pulled completely toward the propellant side of the tank (i.e., completely evacuated). As the propellant enters the tank, the diaphragm buckles into its reversed position. This buckling can occur in a random direction and leads to some uncertainties in the diaphragm ultimate shape. The diaphragm is stiff enough, however, to prevent the fluid from settling into its lowest energy state in the static 1-g environment. The properties of the diaphragm are as follows: tensile strength $= 1.1601 \times 10^6$ kgf/m^2, elongation $= 260\%$, tensile modulus (psi, at 100 elongation) $= 8.4368 \times 10^6$ kgf/m^2, hardness $=$ 90 points, Poisson's ratio and damping properties are unknown, tensile strength change $= -20\%$, and elongation change $= -20\%$. The last two properties represent the elastomer properties after 96 h of exposure to hydrazine at 160°F. In the preliminary evaluation phase of the spin drop test, the scaling of the tensile and bending stiffness of the model diaphragm had to be considered. The spin drop test was conducted on a 1:3.5 reduced model of the Star37FM motor attached to the casing containing the DS1 vehicle with tank full. The Young's modulus for the membrane material is 8.2259×10^5 kg/m^2 for the full-scale diaphragm and 1.7577×10^7 kg/m^2 for the scaled diaphragm. The diaphragm is flexible, but nearly inextensible in its reversed position, that is, at maximum liquid fill level (87.5%). The equilibrium shape of the membrane at maximum liquid fill level is close to axisymmetrical about the $+Z$ axis. This axisymmetry tends to improve the more the tank is full. The equally important issue of scaling down the diaphragm damping properties remains open, although its effect is unknown and intuitively of less magnitude than that of the stiffness.

The damping ratio can be expressed as a nondimensional function of diaphragm stiffness and tank diameter for small oscillations.[23,24] We make the assumption of using data developed for clean tanks (without diaphragm) of diameter d to obtain the fixed pendulum mass m_0, the moving (slosh) mass m_s, and the pendulum length l_s. We also use the data obtained for a 0.5207-m-diam tank with 0.254–0.762-mm-thick diaphragms to extrapolate and to determine the diaphragm stiffness and damping for the DS1 diaphragm.[23,24] Because damping increases with increasing diaphragm thickness for spherical tanks,[23,24] these estimates of damping are conservative. The stiffness and damping coefficients for the slosh pendulum can be computed as[5,6] $k = 0.30 m_s 1^2 (\omega_1 g)^2$ and $c = 0.22 m_s 1^2 \omega_{1g}$. We derive the slosh parameters, that is, slosh mass, slosh pendulum length, and slosh pendulum hinge point, based on data obtained from Abramson's report[7] for a spherical tank of radius d with no PMD. An important assumption to keep in mind is that the charts from Abramson's report[7] are derived assuming a horizontal acceleration field, instead of a centrifugal acceleration field. There is no slosh analysis chart reported in the literature assuming as external excitation a uniform rotational acceleration field. Given the 87.5% fill factor, the chart in Abramson's report[7] (p. 206) provides the following parameters: mass of full tank $m_{\text{full}} = (\frac{4}{3})\pi\rho_f d^3 = 28.70$ kg; effective mass $m_t = \rho_f \pi h^2 [d - (h/3)]$; undamped frequency $\omega_0 = \sqrt{(g/d)} = 6.8511$ rad/s; $\omega_s = 2.335\omega_0 = 15.997$ rad/s; $m_s = 0.075 m_t = 2.0686$ kg; $l_s = 0.335d = 0.07002$ m; hinge point location from tank bottom $l_h = 0.50$ d; rest mass $m_0 = m_{\text{full}} - m_s = 26.631$ kg; and rest mass location $l_0 = 0.99d$. Note that the rest mass is so high because the fill factor is very high, approximating the problem to that of a fully filled spherical tank. Consequently, we assumed the rest mass and the pendulum hinge point to be located at the tank center. The frequency parameter used in Stofan's chart[23,24] turns out to be $\omega_s \sqrt{(d/g)} = 2.335$. As a function of diaphragm thickness, linear extrapolation shows the damping ratio to be as in Table 2. Consequently, the stiffness and damping coefficients for this configuration become $k = 3.403$ N/m and $c = 0.03165$ Ns/m, respectively.

Table 2 Damping ratio of elastomer diaphragms vs diaphragm thickness

Thickness, mm	Damping ratio
0.254	0.27
0.508	0.38
0.762	0.42
1.52	0.73

Dynamic Analysis and Nutation Time Constant Prediction

A nonlinear simulation was carried out of the slosh pendulum model mounted on a rigid spacecraft (as shown in Fig. 4) for the purpose of determining the nutation time constant explicitly. The model is nonlinear because a multibody model is used. Because the nutation time constant is an output of a linearized analysis, it is estimated by means of exponential fitting to the output of the nonlinear program. The nonlinear model represents the problem as a free-floating rigid body connected to a point mass by a universal joint. The system is initially spinning about one axis at 62.3 rpm, and an initial nutation angle is given. The simulation is run for the two cases of preignition and burnout mass properties, and the trend of nutation angle is observed in time. The simulation model features the following elements: 1) a rigid spacecraft body with six degrees of freedom (no flexibility); 2) rigidly connected variable mass rigid solid rocket body; and 3) a viscoelastic pendulum model (two degrees of freedom) for the hydrazine moving mass inside the diaphragm tank. The viscoelastic parameters take into account the membrane dynamics. To derive the equations of motion, we used a projection method, which combines the generalized d'Alembert's principle[25] with a coordinate free approach.[26] Each body is represented by a rigidly attached basis (vectrix, in matrix representation[26]) denoted by F_k, where k denotes the body index. Because we use a universal joint at Q, the position of P with respect to Q can be written as ${}^Q\boldsymbol{r}^P = l_s \boldsymbol{g}_i$, with $\boldsymbol{g}_i = (c\varphi c\theta)\boldsymbol{b}_2 + (c\varphi s\theta)\boldsymbol{b}_3 + (s\varphi)\boldsymbol{b}_1$, and the angular velocity of P in N is ${}^N\boldsymbol{\omega}^P = (\omega_2 + \dot{\varphi}\sin\theta)\boldsymbol{b}_2 + (\omega_3 - \dot{\varphi}\cos\theta)\boldsymbol{b}_3 + (\omega_1 + \dot{\theta})\boldsymbol{b}_1$. The linear velocity of P in N is ${}^Q\boldsymbol{v}^P = {}^N\boldsymbol{v}^O + {}^N\boldsymbol{\omega}^B \times \boldsymbol{h} + l_s F_b^T(\tilde{\boldsymbol{\omega}}\tilde{\boldsymbol{g}}_i + \dot{\theta}\tilde{X}_T + \dot{\varphi}\tilde{X}_F)$, where a superposed tilde denotes the skew-symmetric operator and $X_T = (-c\varphi s\theta)\boldsymbol{b}_2 + (c\varphi s\theta)\boldsymbol{b}_3$ and $X_F = (-s\varphi c\theta)\boldsymbol{b}_2 + (-s\varphi s\theta)\boldsymbol{b}_3 + (c\varphi)\boldsymbol{b}_1$.

With this information, we are ready to extract the partial linear and angular velocities,[25] and we have chosen as generalized speeds the quantities v, ω, $\dot{\theta}$, and $\dot{\varphi}$, respectively. The entries of the inertia matrix M of a system of Nb bodies can be obtained as (the index k represents both the body frame and center of mass of kth body)

$$m_{rs} = \sum_{k=1}^{Nb} \left(m_k {}^N\boldsymbol{v}_r^k \cdot {}^N\boldsymbol{v}_s^k + {}^N\boldsymbol{\omega}_r^k \cdot I_k {}^N\boldsymbol{\omega}_s^k \right) \tag{1}$$

The equations of motion in the generalized speeds $\boldsymbol{u}$ can be written as $M\dot{\boldsymbol{u}} = \tau$, where

$$\tau_r = -\sum_{k=1}^{Nb} \left({}^N\boldsymbol{v}_r^k \cdot F_t^k + {}^N\boldsymbol{\omega}_r^k \cdot T_t^k \right) \tag{2}$$

and $F_t^k = m_k \boldsymbol{a}_t^k - F_e^k$, and $T_t^k = \boldsymbol{I}_k \alpha_t^k + {}^N\boldsymbol{\omega}^k \times I_k {}^N\boldsymbol{\omega}^k - T_e^k$. Here, a_t^k and α_t^k denote the linear and angular acceleration remainder terms (second total accelerations minus contribution to inertia matrix, i.e., nonlinear gyroscopic term). The external torque on the pendulum is given by $T_e = n_\varphi s\theta \boldsymbol{b}_2 - n_\varphi c\theta \boldsymbol{b}_3 + n_\theta \boldsymbol{b}_1$, where $n_\theta = -k\theta - c\dot{\theta}$ and $n_\varphi = -k\varphi - c\dot{\varphi}$ are the viscoelastic reaction torques. The rotation of the base body is parameterized by the unit Euler parameters (quaternion) $\boldsymbol{q}$. Table 3 shows the features of the simulation model.

The system is simulated starting from an initial nutation angle of 0.1 deg. The results show that the two nutation time constants are 1590 s for preignition and 1990 s for burnout, for the given parameters of the spacecraft and hydrazine slosh model. Figure 5 depicts the nutation angle at ignition and burnout vs time showing the sensitivity to different center of mass locations. These numbers are significantly different than those that the energy-sink analysis predicted without including the effect of the diaphragm. Therefore, we conclude that the results of the slosh pendulum model show no danger of instability. Because the nonlinear slosh dynamic model is more detailed than the energy sink analysis, it is also more realistic.

Table 3 Features of simulation model

Model features	Included vs not included
First sloshing mode	Modeled
First-order liquid bulk motion mode	Modeled
Inertial wave modes	Not modeled
Boundary-layer dissipation at tank walls	Not modeled
Froude-number effects	Not modeled
Fluid-structure interaction model	Through joint reactions
Diaphragm elasticity model	Lumped static stiffness
Diaphragm dissipation model	Unknown, assumed damping coefficient
Used computational-fluid-dynamics analysis to improve model	No
Postprocess to get NTC	Fit exponential to line
Pendulum model for slosh	Present
Rotor model for bulk	Not present
Dissipation in rotor model	Unknown, assumed damping coefficient
Variable fill factor	Included
Tank offset from vehicle's c.m.	Included
Star 37 inertial model	Present
Star 37 mass depletion vs time	Present
Nutation control system model	No
Tank shape geometry	Obtained from tables derived from horizontal shaking tests (possibly Abramson's charts); valid only for slosh

The results shown in Figs. 5a and 5b assumed a perfectly balanced spacecraft, and the center of mass location (in spacecraft coordinates) was at 0.2573 m along the Z axis (no X or Y components present). However, subsequent mass properties changes resulted in a slight center-of-mass offset. The new center of mass location is at 0.269 m along the Z axis, -0.65 mm along the X axis, and -0.0094 m along the Y axis. Some simulations have been run incorporating this new change in the preburn and burnout cases, and the results are shown in Figs. 5a–5f. The new (computed) nutation time constant is about 900 s (preburn) and 1450 s (burnout). What we can infer is that the presence of an offset of the center-of-mass along the X and Y axes starts a wobbling motion of amplitude less that 1 deg, superimposed on the nutational instability typical of a prolate spacecraft. The wobbling remains superimposed, because it is not damped, being equivalent to spinning about a different geometrical axis. Eventually, but only over a long time, is the nutation growth visible in the plot of nutation angle vs time. Note that in the preceding case, that is, when the center of mass is on the Z axis, the wobble angle is exactly zero, and the attitude motion is governed by the nutational instability, induced by the slosh motion, alone. In the new case, the estimated wobble angle is 0.30 deg in the preburn case, and 0.24 deg in the burnout case. We see that, besides the wobble angle induced by the center-of-mass offset, there is an additional contribution to the amplitude of the nutation angle, which is caused by the wobble amplification induced by the motion of the slosh mass: its effect is similar to having one flexible mode. If, in addition, we assume that the spacecraft has been balanced, but imperfectly, so that a residual offset is left along the X and Y axes (in this case, an offset of 6×10^{-4} mm along the X and of -6×10^{-4} mm along the Y axes), the result is still different, implying that a very slight offset has also the potential of initiating a wobbling motion. In this case, this wobbling motion is of much smaller amplitude. The nutation time constants are practically the same as in the perfectly balanced case, but with some slight wobbling superimposed (1500 s for preburn, 1900 s for burnout). The estimated wobble angle is 0.035 deg for the preburn case and 0.028 deg for the burnout case. In this case, the wobble amplification caused by slosh motion is much less than in the preceding case. At this point we deem it necessary to quote El-Raheb and Wagner[27]: "Using an equivalent dynamic pendulum model . . . it is impossible to achieve such a simplified equivalence for rotating tanks where Coriolis accelerations and vorticity prevail. Therefore, a pendulum model can only give an incomplete fluid behavior representation." Table 4 summarizes the results.

Table 4 Numerical computation of time constant and wobble angle for different center of mass offsets

Configuration (showing c.m. location in body frame)	Wobble angle, deg	Time constant, s
Preburn (no offset)	0	1590
Burnout (no offset)	0	1990
Preburn [−0.0041 −0.0094 0.2690]	0.30	900
Burnout [−0.0041 −0.0094 0.2690]	0.24	1450
Preburn [0.0008 −0.0008 0.2690]	0.035	1560
Burnout [0.0008 −0.0008 0.2690]	0.028	1960

In conclusion, the effect of having a c.m. off the Z axis is to reduce the time constant (even a slight offset causes this reduction, showing how sensitive the spacecraft is to imbalance) and to induce a wobbling motion of max amplitude of 0.6 deg in the preburn case and a maximum amplitude of 0.4 deg in the burnout case. The wobbling motion is also amplified to some degree by the inertial loading imposed by the moving slosh mass, which, from a dynamical point of view, is equivalent to having an additional flexible mode in the system. Nevertheless, these nutation time constants are still well above the minimum requirements, and the wobbling motion is of very small amplitude.

Spin Drop Tests

The drop test facility used by Jet Propulsion Laboratory and run by Jon Harrison is at Applied Dynamics Laboratories. The facility is located in a three-story building especially designed for all aspects of drop-test model research, design, construction, testing, and data reduction and analysis. The basement area is used for storage of model construction materials; the first floor is used as a machine shop; and the second floor is the office, data reduction, and computer area. The drop tower is located at one end of the building. The hardware specifically related to drop testing includes the following: spin-up/release mechanism, tower and catch box, and telemetry and data processing system. Details of the facility are given in Ref. 6. Figure 6 shows details of the scaled tank and diaphragm. The dynamics induced by the xenon and hydrazine tanks were tested independently, in different phases of the test program, because the xenon tank (tested in phase 1) contained a gas, whereas the hydrazine tank (tested in phase 2) contained a liquid and a deformable element inside. The drop tests for the hydrazine tank and for the xenon tank give separately two different time constants, τ_{Xe} and τ_{Hy}, which are combined to give the final system's nutation time constant as $1/\tau = 1/\tau_{Xe} + 1/\tau_{Hy}$.

Xenon-Tank Drop-Test Program

In this phase of testing, the drop tests for the xenon tank used a drop-test model with a 1/5-scale model of the xenon tank filled with an appropriately scaled liquid. Along with predicting the nutation time constant for the nominal parameters, the main effort of the test program was to uncover any fluid resonances that might exist. The search was limited to inertia ratios approximately 10% above and below the nominal values with an increment of approximately 0.01. Ballast weights on the model were adjusted to change the inertia ratio. The time constant for the full-scale vehicle was computed by scaling the model results using scaling laws based on the energy-sink assumptions. The kinematic viscosity for any load was approximately 0.054 centistokes. The design of the model was driven by the need to simulate the xenon fluid accurately. The two scaling laws that are relevant are the Mach number ($d\Omega/V$) and Reynolds number ($d^2\Omega/\nu$). The full-scale Mach number was between 0.0055 and 0.0124. This is so much less than one that compressibility effects are of much less importance than viscosity effects. Therefore, the model, which uses a liquid to represent the xenon, was designed to match Reynolds number accurately. The xenon fluid has a very

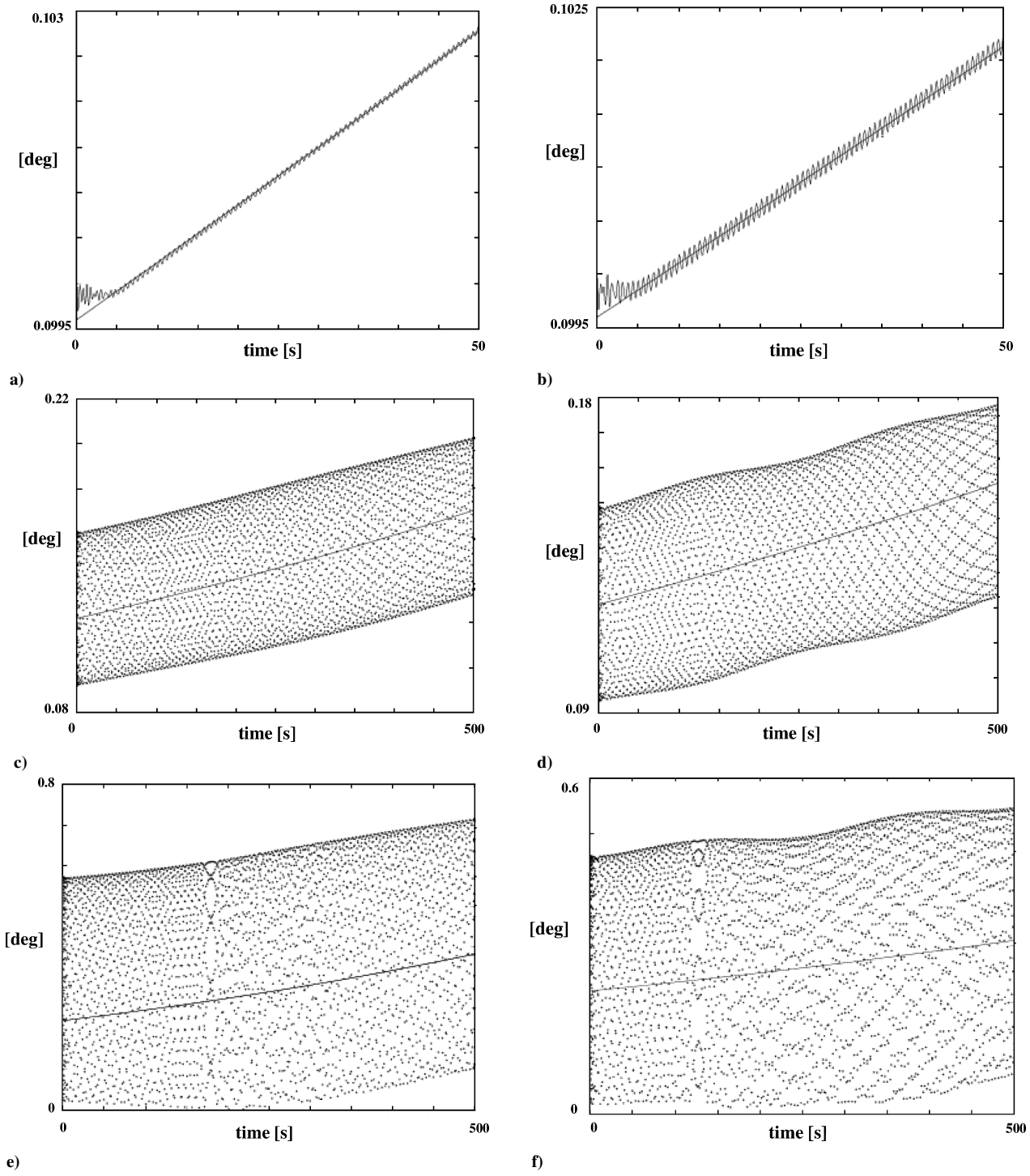

Fig. 5 Nutation angle (deg) at ignition (a, c, e) and burnout (b, d, f) vs time with center of mass at [0; 0; 10.2573] m (first row), with center of mass at [0.0008; −0.0008; 0.269] m (second row), and with center of mass at [−0.0041; −0.0094; 0.269] m (third row).

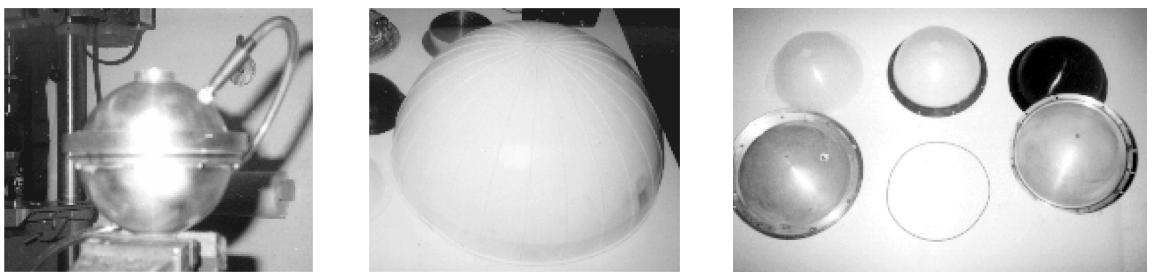

a) b) c)

Fig. 6 Photographs showing a) the Deep Space 1 scaled tank being filled with water before the spin drop test, b) the scaled diaphragm to be placed inside the Deep Space 1 scaled tank, and c) the components of the Deep Space 1 model tank with diaphragm.

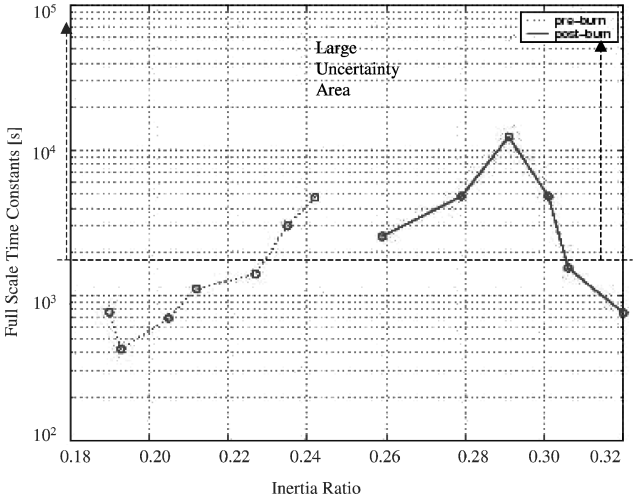

Fig. 7 Full-scale time constants in the pre- and postburn cases vs inertia ratio for the xenon tank. (The arrows indicate the large area of uncertainty in the measurements.)

low viscosity, which in turn requires a very low-viscosity model liquid. The liquid used was a 1,1,2 trichloroethane. It has a density of 1.44 kg/liter and a kinematic viscosity of 0.83 centistokes (1/12 that of water). With a length scale of 1/5, the Reynolds numbers exactly match at a model spin rate of 2300 rpm. This speed was used for all tests. No data were found for the velocity of sound in 1,1,2 trichloroethane, but, based on data for other similar liquids, it was estimated that the value was approximately 1500 m/s. The Mach number for the model was, therefore, approximately 0.01, which was close to the full-scale value. Because the Mach numbers for the model and the full-scale vehicle were 1) so much less than one and 2) so closely matched, it was felt that the model liquid accurately simulated the xenon fluid, a compressed gas. Based on the energy-sink assumptions, the scaling law used to scale the data for the model and full-scale vehicle was $\rho d^5 \Omega \tau / J =$ constant. The results from the tests are summarized in Fig. 7. These test results indicated full-scale preburn time constants in excess of 1000 s for all inertia ratios above 0.21. Below 0.21 inertia ratio, the data indicated that a liquid resonance mode existed at approximately 0.19 inertia ratio. The preburn and postburn results are plotted in Fig. 7. There is significant uncertainty in the data for model time constants above about 5 s (area enclosed within dotted lines). This was the reason for the scatter in the long time constant preburn data, as well in the postburn data. Even though all of the postburn time constants were long, the data suggested that another resonance mode can exist above inertia ratio 0.33. In conclusion, the nutation time constant considering the presence of the xenon tank only was in excess of 1000 s, which means that the xenon gas behaved almost like a solid lump, rigidly connected to the tank walls.

Hydrazine-Tank Model Diaphragm

In this phase of the testing, analytical scaling laws were developed that define the parameters of the model diaphragm. Three different elastomeric compounds were developed, and several diaphragms were made from each type of material. Depending on the material used, the correctly scaled model spin rate was between 870 and 1300 rpm. The diaphragm was successfully installed in the tank, moved into the reversed position, and the tank filled. Many drop tests were performed without any case of leakage or diaphragm breakage. With the tank fill fraction at approximately 85%, the diaphragm appeared to be slightly stretched and quite rigid. The measured time constants were extremely long. Some tests were run at lower fill levels, and these resulted in shorter time constants. Presumably, this was caused by wrinkles or flexing in the diaphragm when it was not stretched. The model tested had the mass center relatively close to the tank center. Particularly in the preburn state, the mass center to tank center distance was quite large. There was a strong possibility that this lever arm would powerfully drive the liquid/diaphragm system and cause short nutation time constants even at high fill levels. The remainder of this section will discuss the scaling laws and model diaphragm in more detail.

A detailed analytical study of the equations governing the flexible diaphragm deflection as a result of the spinning liquid was performed. This analysis resulted in the following diaphragm scaling laws, which are dimensionless ratios that must be preserved for both the model and the full-scale vehicle: H/R, defines the model diaphragm thickness; and $E/\rho R^2 \Omega^2$, defines the relationship between model spin rate and diaphragm modulus of elasticity. It was assumed that Poisson's ratio is reasonably well matched if the model and the full-scale diaphragm materials are similar. The full-scale parameters were as follows: $R = 0.2096$ m, $H = 0.0017$ m, $\rho = 1007.5$ kg/m^3, $\omega = 60$ rpm, and $E = 8.4368 \times 10^5$ kgf/m^2. The values for E (full-scale and model) were obtained by measuring the deflection η of a sample of material. The sample was suspended on two knife-edge supports (separation l), and a force W was applied. The modulus of elasticity was calculated as $E = Wl^3/4\eta bH^3$. A model tank of radius 0.0603 m was used with water simulating the fuel. The model parameters based on the scaling laws were therefore $H = 0.0047$ m, $\Omega/E = 36.5$ (Ω in revolutions per minute, E in pounds/square inch). The inertia ratio used for the preburn (postburn) drop tests was 0.222 (0.296).

The design of the model diaphragm was driven by two requirements: 1) accurate geometric scale, including thickness and details of the ribs; 2) and the modulus of elasticity sufficiently high to allow testing in the spin speed range of 1000–2000 rpm. Spin speeds of this magnitude usually give enough nutation cycles for accurate drop-test results. The decision was made early on in the program to develop an injection mold. The mold consists of male and female hemispherical surfaces, which are moved into close proximity, separated by the desired diaphragm wall thickness of 0.475 mm. In this process, plastic pellets are placed in a hopper, heated to the melting point, and the fluid injected under high pressure. The material enters the hemispherical cavity at the pole, flows around the surface, and exits at the rim of the equator. The excess material (flash) is later trimmed off. The desirable aspect of injection molding is that there is a wide range of plastics available. Therefore, at least potentially, diaphragms of virtually any desirable stiffness could be manufactured. Another important reason that an injection mold was chosen is that it can also be used for compression molding using rubber. In compression molding the raw rubber material is inserted between the two mold halves, and they are squeezed together. This compresses the rubber and forces it to fill the mold cavity. The part is then removed and cured at high temperature. This vulcanizing process changes the internal structure of the material and increases the stiffness. The first diaphragms made used low-density polyethylene in an injection process. It proved to be extremely difficult to produce a whole diaphragm using this process, although eventually about six accurate parts were made. Hundreds of parts were discarded because only part of the mold was filled. It was difficult to keep the two halves of the mold in the desired relative orientation as the molten plastic was injected as a result of hydraulic action shifting the mold and tight tolerances dictated by the thin (0.475 mm) desired wall section. About three parts were made by using a higher-density polyethylene, but these were even more difficult to obtain and were so stiff that the diaphragm could not be reversed (turned inside out) without breaking. There were no breakage problems with those made from the low-density material, and these were used for all of the drop tests. They have a modulus of elasticity of 2.8123×10^7 kgf/m^2, resulting in a model spin speed of 1200 rpm. After the injection molded parts were made, the compression molding process was used with rubber compounds specially blended for this project. Different proportions of styrene and natural rubber are blended to create materials of varying stiffness. Two such blends were used for this project, resulting in values for E of 1.4624×10^7 and 3.1498×10^7 kgf/m^2. Higher stiffness rubber diaphragms were adopted for subsequent tests for the following reasons: 1) the compression molded rubber units were easier to manufacture in case more were needed; 2) for a given modulus of elasticity, the rubber diaphragm appeared to be

deformed more readily than the polyethylene diaphragm without breaking; 3) because the full-scale diaphragm was made out of a rubber compound, it was assumed that the rubber model diaphragm would be more likely to match Poisson's ratio.

Scaling of Fuel-Membrane-Gas System in a Rotating Tank

This analysis describes in more detail the steps that have led to the numbers just indicated. The analysis was done to identify the way to correctly scale the elastic properties of the diaphragm, that is, axial and bending stiffness, and to determine whether the Poisson ratio needs to be scaled as well. The analysis considered a spinning rigid tank, an incompressible inviscid fluid in the tank, and an elastic membrane modeled as a shell. Because the output of this analysis would have identified the correct stiffness of the scaled membrane, before manufacturing, and there was uncertainty on the manufacturing process, the possibility existed of having to deal with a composite shell, made of two layers. The quantities involved in this scaling procedure are Ω, H, R, J, ρ, p, E_1 (E_2), H_1 (H_2). Then, the tensile stiffness becomes $E_F H_F = E_1 H_1 + E_2 H_2$, and the bending stiffness becomes $E_M H_M^3 = E_2 H_2 [H_2^2 + 3H_1(H_1 + H_2)] + E_1 H_1^3$, Introducing the ratios $\alpha = R_{\text{test}}/R_{\text{fullscale}}$, $\beta = \Omega_{0\text{test}}/\Omega_{0\text{fullscale}}$, $\gamma = \rho_{\text{testliquid}}/\rho_{\text{fuel}}$, the ratios (or nondimensional numbers) that must remain unchanged for the governing equations to remain unchanged are $J/(\rho R^5)$ to satisfy the momentum equilibrium of the rigid body plus the tank and fluid; $p/(\rho R^2 \Omega_0^2)$ to satisfy the Euler equation for the incompressible, inviscid fluid in the tank; $pR/(E_F H_F)$ to satisfy the radial equilibrium of a shell element; and $(E_M H_M^3)/(R^2 E_F H_F)$ to satisfy the moment equilibrium of a shell element. The last two also reduce to the following ones (after recombination with the first two): $(E_f H_F)/(\rho R^3 \Omega_0^3)$ and $(E_M H_M^3)/(\rho R^5 \omega_0^2)$.

With these definitions, the tank diameter in the test model becomes $d_T = \alpha d$, the spin rate Ω_{0T} in the test model becomes $\Omega_{0T} = \beta \Omega_0$, the fuel density ρ in the test model becomes $\rho_T = \gamma \rho$, the spin inertia J in the test model becomes $J_T = \alpha^5 \gamma J$, the membrane tensile stiffness Eh in the test model becomes $E_F H_F = \alpha^3 \beta^2 \gamma EH$, and the bending stiffness EH^3 in the test model becomes $E_M H_M^3 = \alpha^5 \beta^2 \gamma EH^3$. Given the full-scale values of $E = 8.4368 \times 10^5$ kgf/m^2, $\nu = 0.49$, $H = 0.1651$ mm, $d = 0.4191$ m, $\Omega_0 = 60$ rpm, and $\rho = 999.1779$ kg/m^3, the scaling can be done following three approaches. First, increase the Young's modulus, so that both the tensile and bending stiffnesses scale properly. In this case, $d_{\text{test}} = 0.1207$ m, $\Omega_{0T} = 750$ rpm, $\alpha = 4.75/16.5$, $\beta = 750/60$, $H_T = 0.475$ mm, and $E_T = 1.0926 \times 10^7$ kgf/m^2. Second, consider a composite shell, for which one obtains $d_{\text{test}} = 0.1207$ m, $\Omega_{0T} = 58$ rpm, $H_1 = 0.33$ mm, $E_1 = 8.4368 \times 10^6$ kgf/m^2, $H_2 = 0.4826$ mm, and $E_2 = 8.4368 \times 10^5$ kgf/m^2. Third, consider the shell material to be the same as in the full-scale tank, scale the thickness so that the bending stiffness is properly scaled, and accept the improperly scaled tensile stiffness. Then, with $d_{\text{test}} = 0.1207$ m, $\Omega_{0T} = 750$ rpm, $E = 8.4368 \times 10^5$ kgf/m^2, $H_T = 1.1176$ mm, $EH_T = 942.8968$ kgf/m, $\alpha = 0.2280$, $\beta = 12.5$, and $\alpha^3 \beta^2 EH = 1746.2$ kgf/m.

The strain components in the plane tangent to the middle surface of the shell have the form $\varepsilon_{ij} = A_{ij} + B_{ij}(\zeta/R)$. Assuming negligible stresses through the thickness (i.e., σ_{zz}), the stress components have the form $\sigma_{ij} = [E/(1-\nu^2)][C_{ij} + D_{ij}(z/R)]$. With these expressions for strain and stresses, the internal force resultants take the form $F_{ij} = [(EH)/(1-\nu^2)]C_{ij}$, and the internal moment resultants take the form $M_{ij} = [(EH)/(1-\nu^2)]D_{ij}$. Therefore, if the size is scaled and Poisson's ratio is held fixed, E, H, and the other quantities of the system such as spin rate can be scaled in such a way that the shape of the deformed middle surface is the same in the test as in the actual vehicle. This scaling procedure was used to manufacture the scaled diaphragms for use in the drop tests.

Energy-Sink Approximation and Scaling

Energy-sink analyses have been done for a long time in spacecraft dynamics[26]; however, their prediction is not believed to be very accurate in the case of diaphragm tanks on spinning spacecraft because they are extremely conservative. These analyses, however, hold under the following assumptions: 1) the spacecraft contains a tank completely filled with liquid, 2) the liquid does not constitute a large fraction of the spacecraft mass, 3) no liquid motion resonances occur, and 4) no PMD exist. In this case, τ can be estimated as $\tau = [J(1-\beta)\Omega^2]/(G/\theta^2)$. To be of any use, the energy-sink model needs a good model for G, which in our case is very difficult to obtain. Nevertheless, a modification of the last equation is possible to account for the effect of diaphragm elasticity and viscosity. Obviously, the more complex details of inertial wave resonances, and other fluid-structure interaction modes, are neglected in this analysis. It only captures the effect of existing dissipative elements, which somehow can be modeled. We need to find the variables upon which the energy dissipation rate per unit nutation angle squared depends, that is, the functional dependence of G/θ^2. In the simplest case of a spherical tank with no diaphragm and assuming[28] $G/\theta^2 = 1.4 m_f \Omega^3 R^2 / Re^{1/2}$, the energy-sink analysis gives an initial estimate for the nutation time constant of $\tau = 25{,}354$ s at ignition and of $\tau = 14{,}660$ s at burnout. For an on-axis diaphragm tank, this quantity would presumably depend on (using MKS fundamental units) 1) spin rate ω in rad/s, 2) nutation frequency $\lambda = (1-\sigma)\Omega$ in rad/s, 3) fluid mass m_f in kg, 4) fluid density ρ_f in kg/m^3, 5) fluid viscosity μ_f in kg/ms, 6) axial offset of tank center from spacecraft center of mass z in m, 7) tank diameter d, 8) tank shape factor S (spherical, cylindrical, etc.), 9) tank FF, and 10) external acceleration field g in m/s^2.

We can model the diaphragm as a thin shell of density ρ_d, thickness H_d and Poisson's ration ν. The extensional stiffness is $\Lambda_d = EH/(1-\nu^2)$, the shear stiffness is $\Gamma_d = GH$, whereas the bending stiffness is $\Sigma_d = EH^3/[12(1-\nu^2)]$. Therefore, accurate scaling should include these three stiffness coefficients. The membrane damping coefficient c_d, proportional to a stress divided by strain rate, can characterize the viscoelastic properties of the disphragm. However, $\Gamma_d = \Lambda_d/2$, and Λ_d is proportional to Σ_d/H^2;

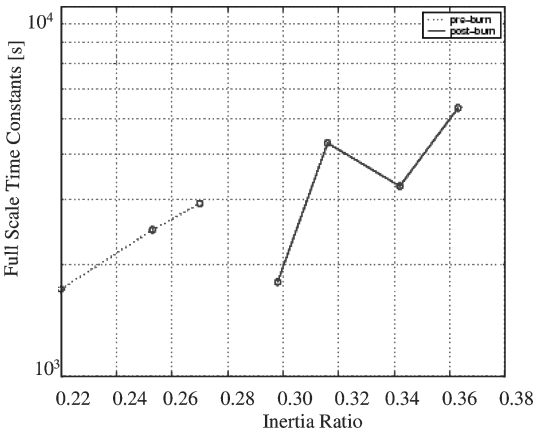

Fig. 8a Full-scale pre- and postburn time constants vs inertia ratio for the hydrazine tank.

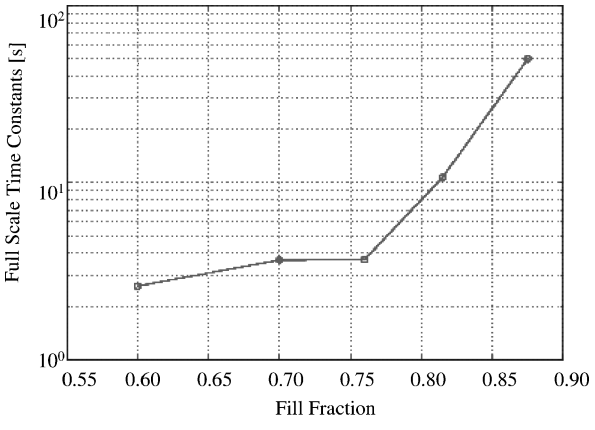

Fig. 8b Full-scale time constants vs fill fraction for the hydrazine tank.

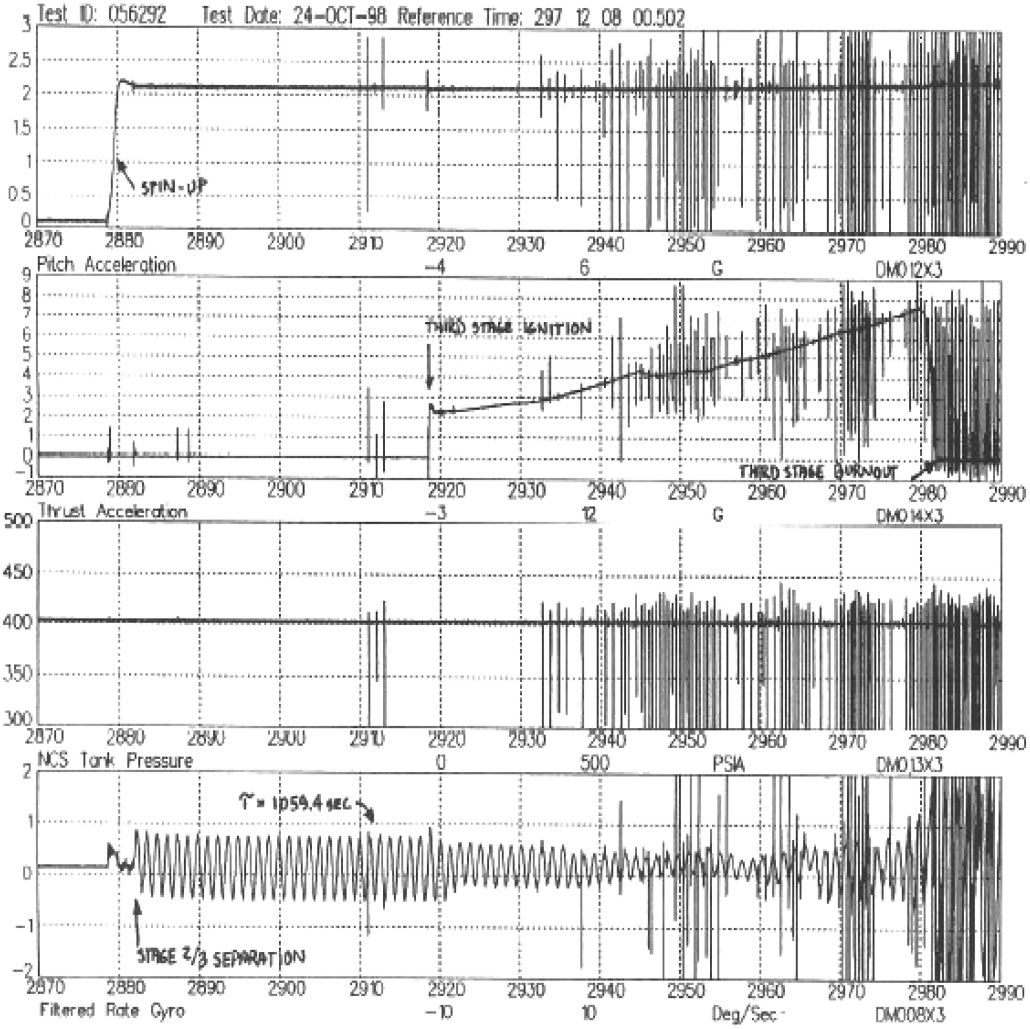

Fig. 9a Pitch acceleration, thrust acceleration, NTC tank pressure, and filtered rate gyro vs time during Star-37 ignition (courtesy of James Corbo, Boeing Astronautics).

hence, we only retain Σ_d. Using the techniques of dimensional analysis and introducing the arbitrary constants c_i and exponents p_i, we can write

$$\frac{G}{\theta^2} = \sum_i c_i \Omega^{p_1} \lambda^{p_2} m_f^{p_3} \rho_f^{p_4} \mu_f^{p_5} z^{p_6} d^{p_7} S^{p_8} g^{p_9} \rho_d^{p_{10}} H^{p_{11}} \times \Sigma_d^{p_{12}} c_d^{p_{13}} \nu^{p_{14}} \tag{3}$$

There are 14 dependent variables and three fundamental variables. Hence, Buckingham's theorem says that there remain 11 nondimensional groups of variables that define the problem (perhaps even less than 11 because there are several similar groups, i.e., length over length, and others). We can rewrite the preceding equation in terms of the fundamental units M, L, and T. Setting the equality of powers, we obtain the identities $p_1 = 3 - p_2 - p_5 - 2p_9 - 2p_{12} - p_{13}$, $p_3 = 1 - p_4 - p_5 - p_{10} - p_{12} - p_{13}$, and $p_7 = 3 + p_5 + 3p_4 - p_8 - p_9 + 3p_{10} - p_{11} - 2p_{12} + p_{13}$. Substituting back, we obtain

$$G\Big/\left(\theta^2 d^2 m_f \Omega^3\right) = f\Big\{(\lambda/\Omega)^{p_2}\left(\rho_f d^3\Big/m_f\right)^{p_4}[d\mu_f/(\omega_s m_f)]^{p_5} \times (z/d)^{p_6}(S/1)^{p_8}(g/(\Omega^2 d)^{p_9}\left(d^3\rho_d\Big/m\right)^{p_{10}}(H/d)^{p_{11}} \times \left(\Sigma_d\Big/\left(\Omega^2 m_f d^2\right)^{p_{12}}(c_d d/(\Omega m_f)^{p_{13}}\nu^{p_{14}}\Big\} \tag{4}$$

The first term inside the functional dependence can be reduced to the inertia ratio σ because the nutation frequency is $\lambda = \Omega(1-\sigma)$. The mass of fluid is equal to $m_f = \rho_f d^3 FF$. Hence the tank fill fraction FF can be considered another dependent variable. The second term can be reduced to FF. The third term can be reduced to $1/Re_f$ (the Ekman number[8]). The sixth term is equal to the Froude number Fr_f. The seventh term can be reduced to ρ_d/ρ_f. The ninth term can be written as $\Sigma_d/(\Omega^2 m_f d^2) = EH^3[12(1-\nu^2)\Omega^2 d^2 \rho_f d^3] = Bo_E/[12(1-\nu^2)](H^2/d^2)$. Finally, the last term can be manipulated as $c_d d/(\Omega^2 m_f) = 1/(Re_E FF)$. Consequently, the nutation time constant for an on-axis diaphragm tank on a spinning body can be rewritten as $\tau = f\sigma(\sigma-1)I/(\rho_f d^5 \omega_s)$, where f is a function defined by $f = f[\sigma, FF, Re_f, Fr_f, Bo_E, Re_E, (z/d), (H/d), (\rho_d/\rho_f), S, \nu]$ and which, in some fashion to be determined yet, will have to be determined experimentally. Notice that the dependency on σ, FF, (z/d), (H/d), (ρ_d/ρ_f), S, ν, Re_f, and Fr_f can be obtained through some computational-fluid-dynamics model, whereas the dependency on Bo_E, Re_E can be determined through a fluid-structure interaction code. In conclusion, a reasonably accurate estimate of the diaphragm effect on a spinning on-axis tank can be obtained analytically via energy-sink analysis.

Hydrazine-Tank Drop-Test Program

In this phase of testing, a newly developed rubber diaphragm was used for all of the tests, allowing the desired fill level of 87.5% to be reached (with the plastic diaphragm originally developed, the maximum fill level was 85%). Models representing the pre- and postburn state were tested at the nominal inertia ratio and for values approximately 10% higher and lower than the nominal. All results show very long time constants. The full-scale time constant was computed by inertia scaling by using the standard scaling law $\rho R^5 \Omega \tau / J$. The scaling was approximately $\tau_{\text{fullscale}} = 98\tau_{\text{model}}$ for the preburn case and $\tau_{\text{fullscale}} = 59\tau_{\text{model}}$ for the postburn case. Figure 8a shows a plot

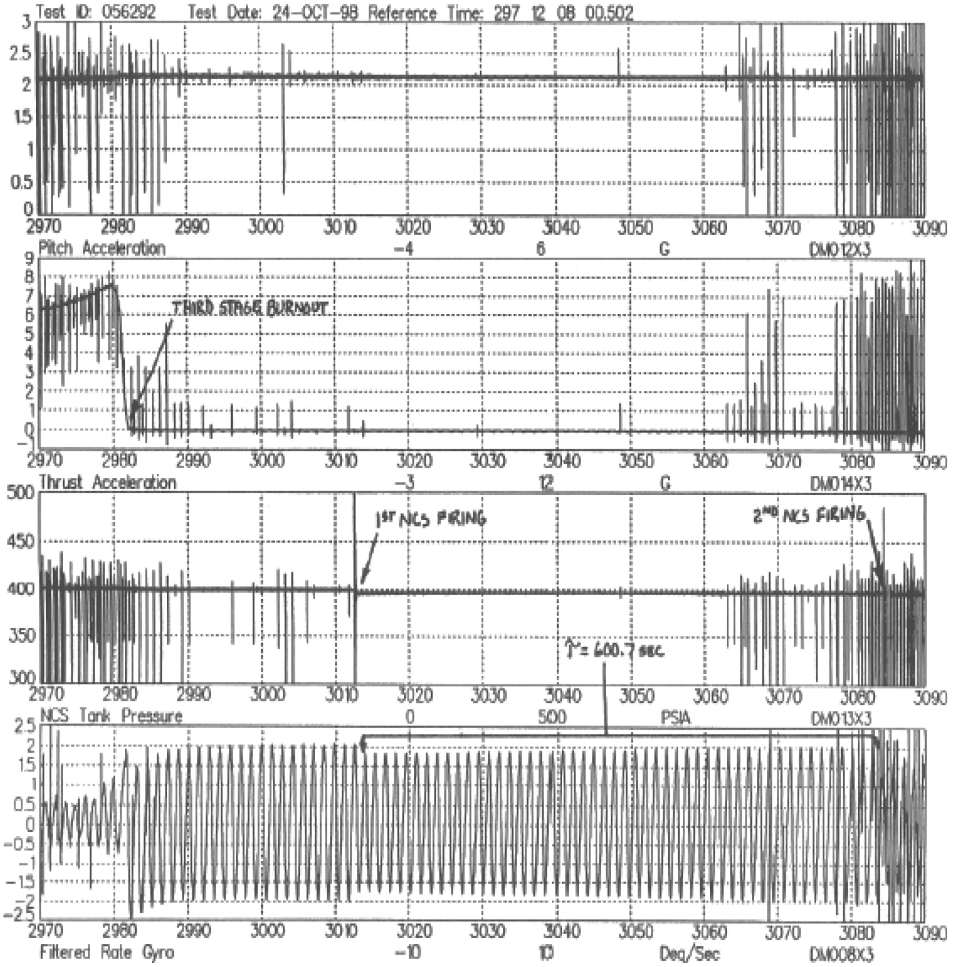

Fig. 9b Pitch acceleration, thrust acceleration, NTC tank pressure, and filtered rate gyro vs time during Star-37 burnout (courtesy of James Corbo, Boeing Astronautics).

of the time constants for the test results in the preburn and postburn cases. For this test program, a high confidence level existed for model time constants shorter than about 5 s. For values longer than 5 s (all test results), there was uncertainty in the results, which explains the scatter in the data. When dealing with very long time constants, as in this test program, it would also be more meaningful to speak in terms of inverse time constant because that reflects the energy dissipation rate more accurately. Finally, Fig. 8b depicts the sensitivity of the nutation time constant to the liquid fill fraction.

Flight-Test Results

Figures 9a and 9b show the pitch acceleration, thrust acceleration, NTC tank pressure, and filtered rate gyro vs time during Star-37 ignition and burnout, respectively. These plots confirm the results of the analysis and testing by showing that, through very long time constants, nutation barely developed in these phases of the DS1 flight.

Conclusions

The conclusions of this paper are as follows. First, several modeling issues have been described, particularly concerning the effect of the membrane in the hydrazine tank. An energy-sink analysis gives an initial estimate for the nutation time constant of $\tau = 25{,}354$ s at ignition and of $\tau = 14{,}660$ s at burnout. We observe that, assuming a perfect mass balance, liquid slosh is probably not an issue in this type of diaphragm tank configuration. The only uncertain dynamic response was in terms of liquid resonances (inertial wave modes), which might have been excited inside the xenon and the hydrazine tanks. Second, to simulate the nonlinear behavior of the spacecraft containing the liquid (hydrazine), the dynamics of a rigid body coupled through a universal joint to a pendulum mass representing the liquid slosh has been analyzed. Despite the uncertainty in diaphragm viscoelastic properties, the results of the analysis show that the nutation time constant is $\tau = 1590$ s at ignition and $\tau = 1990$ s at burnout. The fact that these two numbers are not very different can be intuitively explained because of the very large tank fill factor, which approximates the behavior of this tank to that of a fully filled spherical tank. Third, spin drop tests also confirm a nutation time constant in excess of 1000 s, both in the case of tests done for the xenon tank only and in the case of tests done for the hydrazine tank only. Fourth, flight data report a small number of nutation control system firings and nutation time constants of 1055 s (preburn) and 605 s (postburn), confirming reasonably well the analysis and test results.

Acknowledgments

The research described in this paper was carried out at the Jet Propulsion Laboratory (JPL), California Institute of Technology, under a contract with NASA. The author is grateful to Sam Sirlin, Dankai Liu, and Mike Davis of JPL for financial and intellectual support; to Jon Harrison of Applied Dynamics Laboratories, Inc., for conducting the drop tests; to Carl Hubert of Hubert Astronautics, Inc., for providing useful information on the nutation synchronous mode; and to James Corbo of Boeing Astronautics for providing the flight-test data.

References

[1]Marce, J., "Energy Dissipation In Exosat Tanks—Test Results," Centre National d'Etudes Spatiales, Technical Note, CNES-NT-99, March 1981.

[2]Dodge, F., "Propellant Dynamics and PMD Design for the Near Earth Asteroid Rendezvous (NEAR) Spacecraft," Southwest Research Inst., SWRI Project 04-6297, San Antonio, TX, April 1994.

[3]Hubert, C., "Assessment of MSP Lander Propellant Dynamics During Spinning Operations," Hubert Astronautics, Rept., West Windsor, NJ, Jan. 1997.

[4]Wood, J., "Mars '98 Lander Nutation Time Constant Estimate Issues," VSG-ML-M-0897-003R1, 18 Aug. 1997.

[5]Hubert, C., "Deep Impact Nutation Assessment," Hubert Astronautics, Rept. B2050, West Windsor, NJ, July 2002.

[6]Harrison, J., "Analysis of Spacecraft Nutation Dynamics Using the Drop Test Method," *Space Communications and Broadcasting*, Vol. 5, No. 4, 1987, pp. 265–280.

[7]Abramson, H. N., "The Dynamic Behavior of Liquids in Moving Containers," NASA SP-106, 1966.

[8]Greenspan, H. P., *The Theory of Rotating Fluids*, Cambridge Univ. Press, 1969.

[9]Stewartson, K., "On the Stability of a Spinning Top Containing Liquid," *Journal of Fluid Mechanics*, Vol. 5, No. 4, 1959, pp. 577–592.

[10]Wedemeyer, E. H., "Viscous Corrections to Stewartson's Stability Criterion," BRL Rept. 1325, Aberdeen Proving Ground, MD, 1966.

[11]Alfriend, K. T., "Partially Filled Viscous Ring Nutation Damper," *Journal of Spacecraft and Rockets*, Vol. 11, No. 7, 1974, pp. 456–462.

[12]Cartwright, W. F., Massingill, E. C., and Trueblood, R. D., "Circular Constraint Nutation Damper," *AIAA Journal*, Vol. 1, No. 6, 1963, pp. 1375–1380.

[13]McIntyre, J. E., and Tanner, T. M., "Fuel Slosh in a Spinning on-Axis Propellant Tank: An Eigenmode Approach," *Space Communication and Broadcasting*, Vol. 5, No. 4, 1987, pp. 229–251.

[14]Mingori, L., and Harrison, J., "Circularly Constrained Particle Motion in Spinning and Coning Bodies," *AIAA Journal*, Vol. 12, No. 11, 1974, pp. 1553–1558.

[15]Vanyo, J. P., *Rotating Fluids in Engineering and Science*, Butterworths, London, 1993.

[16]Miles, J., "Free Surface Oscillations in a Rotating Liquid," *Physics of Fluids*, Vol. 2, 1959, pp. 297–305.

[17]Miles, J., and Troesch, B., "Surface Oscillations of a Rotating Liquid," *Journal of Applied Mechanics*, Vol. 28, 1961, pp. 49–96.

[18]Zedd, M. F., and Dodge, F. T., "Energy Dissipation of Liquids in Nutating Spherical Tanks Measured by a Forced Motion Spin Table," AIAA Paper 84-1842, 1984.

[19]Ross, R. G., and Womack, J. R., "Slosh Testing of a Prototype Electric Propulsion Mercury Propellant Tank with Positive Expulsion Diaphragm," AIAA Paper 73-1120, 1973.

[20]Kreis, A., Kurz, A., Klein, M., and Deloo, Ph., "Static and Dynamic Modeling of Diaphragm Tanks," *Proceedings of the Conference on Spacecraft Structures, Materials, and Mechanical Testing*, Noordwijk, The Netherlands, 1996.

[21]Kana, D. D., "Validated Spherical Pendulum Model for Rotary Liquid Slosh," *Journal of Spacecraft and Rockets*, Vol. 26, No. 3, 1989, pp. 188–195.

[22]Kana, D., and Dodge, F., "Preliminary Study of Liquid Slosh in the Tracking and Data Relay Satellite Hydrazine Tanks," Southwest Research Inst., Final Rept. of Project 02-5887, San Antonio, TX, Dec. 1979.

[23]Stofan, A., and Pavli, A., "Experimental Damping of Liquid Oscillations in a Spherical Tank by Positive Expulsion Bags and Diaphragms," NASA TN-D-1311, July 1962.

[24]Stofan, A. J., and Sumner, I. E., "Experimental Investigation of the Slosh-Damping Effectiveness of Positive Expulsion Bags and Diaphragms in Spherical Tanks," NASA TN-D-1712, June 1963.

[25]Kane, T., Likins, P., and Levinson, D., *Spacecraft Dynamics*, McGraw–Hill, New York, 1984.

[26]Hughes, P. C., *Spacecraft Attitude Dynamics*, Prentice–Hall, Upper Saddle River, NJ, 1986.

[27]El-Raheb, M., and Wagner, P., "Vibration of a Liquid with a Free Surface in a Spinning Spherical Tank," *Journal of Sound and Vibration*, Vol. 76, Pt. 1, 1981, pp. 83–93.

[28]Dodge, F. T., "Slosh Investigation," Southwest Research Inst., Final Rept. to RCA, Project 06-1378-101, San Antonio, TX, April 1987.

C. Kluever
Associate Editor